Proceedings of The Thirteenth (2003) International Offshore and Polar Engineering Conference
Honolulu, Hawaii, USA, May 25−30, 2003

ISBN 1−880653-60−5 (Set); ISSN 1098−6189 (Set)

Underwater Landslide Shape, Motion, Deformation, and Tsunami Generation

Philip Watts[1], *Stephan T. Grilli*[2]
[1]Applied Fluids Engineering, Inc.
Long Beach, California, USA
[2]Ocean Engineering, University of Rhode Island
Narragansett, Rhode Island, USA

ABSTRACT

We study underwater landslide shape, motion and deformation at early times. We present experimental and numerical results in a search for general behaviors of tsunamigenic underwater landslides. Our experimental work presents a granular mass moving and deforming down a steep incline. Our numerical work uses a Bingham-like fluid model (BING) to simulate more realistic underwater landslide models. We show that both landslide motion and deformation can be described with theoretical predictions derived for solid blocks. We find that it is possible to reduce our results into analytical expressions for shape, motion, and deformation of coherent features.

KEY WORDS: Landslide; tsunami; shape; motion; deformation; length; thickness.

INTRODUCTION

Underwater landslides present a challenging tsunami generation problem (Grilli and Watts, 1999, 2001; Grilli *et al.*, 2002). On the one hand, the underwater landslide must be treated with care and precision as an accelerating and deforming body. On the other hand, the wave generation problem involves complicated fluid flows and wave behaviors that remain subjects of active research. In this work, we present fundamental analyses of underwater landslide shape, motion, and deformation, with the understanding that these have a direct bearing on the problem of tsunami generation. To be more specific, we study the behavior of underwater slides at early times, as a reasonable starting point in a larger research effort.

The mechanics of moving and deforming bodies is often considered with "relative motion", which decomposes a moving body into the motion of the center of mass, and then the motion and/or deformation about that same center of mass. Based on this conceptual framework, a deforming landslide has a center of mass motion with a given position and velocity. The center of mass motion may also depend on deformation. However, when we discuss this center of mass motion, we are in no way precluding landslide deformation, because that deformation occurs about the center of mass, by definition. Despite this fundamental concept of relative motion, there are few tsunami studies that have considered the center of mass motion of deforming underwater landslides. We propose to do so in this work.

When analyzing center of mass motion, it seems natural that solid block landslides should provide a reasonable starting point for analyses of deforming landslides. One advantage of doing this is that the solid block center of mass motion can be well-defined from laboratory experiments. Besides, Watts (1997) showed through laboratory experiment results that deforming landslides have a center of mass motion that is similar in many regards to that of solid blocks. Therefore, the classical tsunami generation work of Wiegel (1955) and experiments and analytical work by Watts (1998, 2000) should apply to most underwater landslide tsunamis, even though that work was based solely on solid blocks. Computations by Watts *et al.* (2000) using the two-fluid landslide model of Imamura and Imteaz (1995) provide yet another confirmation that the center of mass motion remains similar to that of a solid block. These results motivate the current study, because they suggest that the center of mass motion of an underwater landslide may be a robust and predictable quantity, regardless of deformation.

Watts *et al.* (2000) also found that landslide deformation can contribute to the center of mass motion. Thus, there is a solid block component to landslide center of mass motion, but there can also be a second component to center of mass motion brought about by landslide deformation. Basically, mass can shift forward to form the nose of a deforming landslide, and this shift moves the center of mass forward. Both components of the total center of mass motion can contribute to tsunami generation. Therefore, deformation should always be considered for tsunami generation, although its importance remains poorly assessed, in part because landslide shape evolves in time.

In this work, we study landslide motion and deformation at early times, which is understood to mean: while the landslide is still accelerating and while tsunami generation is still taking place. These two conditions are redundant because one can define the duration of tsunami generation by the characteristic duration of landslide

acceleration (Watts, 1998, 2000). Because we are only interested in landslide motion at early times, it seems reasonable to consider a planar incline with constant slope.

Last of all, in this work , we have chosen to focus on underwater slides, i.e., a subclass of underwater landslides, which is a more general or umbrella term. We will introduce a morphological definition of underwater slides below. Our research technique should apply equally well to other classes of underwater landslides, although we do not endeavor to prove this point here. Instead, we wish to establish that it is possible to describe underwater slide shape, motion, and deformation in the first place.

ANALYTICAL CONSIDERATIONS

Mathematical or analytical equations enable some predictions of underwater slide shape and motion. We would like to analyze our subsequent results within the framework of analytical equations, because these equations offer relationships between fundamental scales and because they can serve to simplify complicated phenomena through the use of simple quantities.

Underwater Slide Shape

At this stage, in our consideration of underwater slide shape, we are interested in the gross features present at the initiation of inertial failure. When viewed as a cross-section from the side, an underwater slide can be characterized by an initial length B parallel to the slope and a maximum thickness T perpendicular to the slope. These two measures of size form a dimensionless quantity called the thickness to length ratio T/B that helps quantify slide morphology. We examined underwater slide records (e.g., Prior and Coleman, 1979; Edgers and Karlsrud, 1982; Schwab *et al.*, 1993; Hampton *et al.*, 1996) for indications of a typical thickness to length ratio. It appears as though underwater slides are grouped around a mean thickness to length ratio of roughly 0.01 to within a factor of two, which implies long and thin mass failures. Another morphological feature of underwater slides is that the mass often travels significant distances from the headwall scar before coming to rest. This indicates a rapid acceleration and large translational velocities. A more detailed morphological classification of an underwater slide may depend on specific mass failure processes that we do not consider here. Regardless, underwater slides are sufficiently common to be of concern as tsunami hazards, perhaps comprising up to half of all tsunamigenic underwater landslides.

Underwater Slide Motion

Watts (1997) considered the forces acting on underwater slides in some detail. Simplified versions of this analysis providing reasonable force balances appear in Pelinovsky and Poplavsky (1996) or Watts (1998), who describe a useful center of mass motion valid at early times. We summarize those results here.

If we assume a planar incline of angle θ for the sake of our current study, then the solution to the balance of inertia, gravity, basal friction, and hydrodynamic drag forces acting on the entire slide bulk becomes

$$s(t) = s_o \ln\left[\cosh\left(t/t_o\right)\right] \tag{1}$$

in which s_o denotes a characteristic distance of motion and t_o denotes a characteristic duration of motion (Watts, 1998, 2000). These two quantities are found from the underwater slide initial acceleration a_o and theoretical terminal velocity u_t according to

$$a_o = \frac{g\left(\gamma - 1\right)\left(\sin\theta - C_n \cos\theta\right)}{\gamma + C_m} \tag{2}$$

$$u_t = \sqrt{\frac{4Bg\left(\gamma - 1\right)\left(\sin\theta - C_n \cos\theta\right)}{3\,C_d}} \tag{3}$$

$$s_o \equiv \frac{u_t^{\,2}}{a_o} \tag{4}$$

$$t_o \equiv \frac{u_t}{a_o} \tag{5}$$

where g is the acceleration of gravity, $\gamma \equiv \rho_b / \rho_w$ is the specific density, ρ_b is the bulk density, ρ_w is the water density, C_m is the added mass coefficient, C_d is the drag coefficient, and C_n is the Coulomb friction coefficient. Eq. 1 is a common analytical solution for free bodies subjected to gravity and form drag at high Reynolds numbers. Eqs. 2-5 are specific to a fully submerged, solid block slide with an approximately parabolic profile.

Eq. 1 is meant solely to capture the correct initial acceleration during tsunami generation, which occurs at early times $t < t_o$ following inertial failure. In fact, this criterion serves as our definition of early time. Given this strict time constraint, our force balance should be sufficient to correctly represent slide center of mass motion. Further, there should be no need for center of mass motion refinement if one is concerned only with tsunami hazards. Indeed, Fig. 1 shows that the first term in the Taylor series of Eq. 1 can provide a reasonably accurate description of slide motion during $t < t_o$ by using only the initial acceleration from Eq. 2. Eq. 3 demonstrates that terminal velocity increases with the square root of slide initial length. However, the slide maximum thickness does not appear explicitly in Eqs. 2-5.

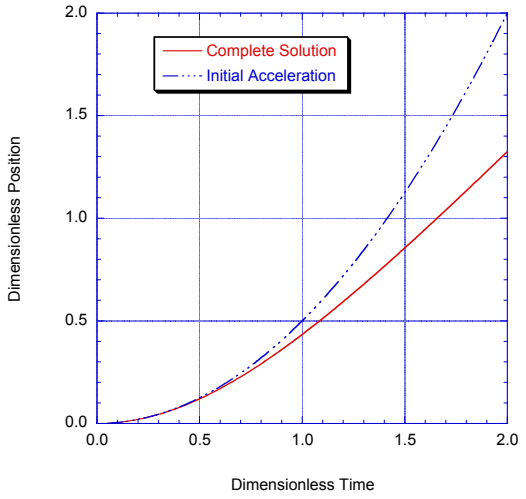

Fig. 1: Comparison of Eq. 1 with the first term in its Taylor series

We suggest the added mass coefficient $C_m \approx 1.76$ and the drag coefficient $C_d \approx 1.53$ obtained from the experimental work of Grilli *et al.* (2002) performed with an ellipsoidal slide shape. However, from

our experience, underwater slide motion is not particularly sensitive to these two coefficients (Watts, 1998). We note that our hydrodynamic drag force depends on slide *thickness* and width, rather than slide *length* and width. Frictional forces along the slip surface may or may not be important in underwater slide motion, depending on the sediment type, the water pressure, the margin history, and the tectonic regime, that all contribute to failure. Given an effective residual shear strength S_u, we calculate a mean Coulomb friction coefficient with

$$C_n = \frac{3\,S_u}{2(\rho_b - \rho_o)gT\cos\theta} \qquad (6)$$

where we have once again assumed a parabolic slide profile. Eq. 6 introduces the slide maximum thickness into the center of mass motion. Consequently, even if sediment retains significant residual strength, progressively thicker slides experience lesser restraint on their motion. The Coulomb friction at lab scale will often be very different from that in the real world. On the one hand, laboratory scale slides will often experience prohibitive Coulomb friction. On the other hand, it would not be surprising to find gravitational forcing much larger than basal friction for a real underwater slide event. This arises because the gravity that accelerates slides is a body force, whereas the basal friction that restrains slides is a surface force, and Eq. 6 indicates that slide volume typically increases faster than basal area.

LABORATORY EXPERIMENT METHODS

We report on a subset of the experimental work of Watts (1997), to which we refer the interested reader for additional details. To be specific, we consider only three trials, carried out with three different granular materials: trial 82 carried out with 3 mm glass beads, trial 81 carried out with 3 mm steel shot, and trial 86 carried out with 3 mm lead shot. Each underwater slide started out with the same triangular shape and bulk volume (Fig. 2), with the primary difference consisting of the bulk density. The tank width and length are not important here. Similar experiments related to tsunami generation by underwater slides have also been conducted by Assier-Rzadkiewicz *et al.* (1997).

Table 1. Granular material properties for laboratory experiments

Material	ρ_s	ρ_b	ϕ	ψ	D
Glass	2563	1935	29˚	6˚	2.96
Steel	7954	5102	28˚	6˚	3.31
Lead	10727	7321	34˚	12˚	3.11

The solid density ρ_s (in kg/m^3) was measured with a specific gravity balance. Almost all spherical particles had solid volume fractions between 0.58-0.61 with the exception of 3 mm lead shot which had a solid volume fraction of 0.65. The bulk density ρ_b (in kg/m^3) was calculated with the solid volume fraction. The internal friction angle ϕ and incline friction angle ψ were determined experimentally for the slide materials. The internal friction angle ϕ governs failure throughout the mass of slide material while the incline friction angle ψ is related to the Coulomb friction of the slide material on the Lucite incline. If the internal friction angle ϕ was being determined, then a random layer of slide material was deposited on a Lucite sheet and held in place by a thin layer of silicone sealant. If the incline friction angle ψ was being determined, then the material was deposited directly onto a Lucite sheet and tested by inclining the sheet until failure. The mean diameter D of the particles (in millimeters) is based on multiple micrometer readings of hundreds of particles. The average results of all measurements are summarized in Table 1.

A material landslide with vertical front face of 85 mm and horizontal top face of 85 mm was initiated by retracting a vertical gate down into a Lucite incline of $\theta = 45$ degrees. The gate motion into the incline was rapid enough to release the granular mass in almost the same shape as when it was initially impounded behind the gate. The downward motion of the gate was necessary to minimize disruption of both the slide material and the water free surface. It is also important to note that retracting the gate must change the state of stress in the slide material regardless of gate shearing: the slide material goes from being supported by a solid retaining wall to being unsupported. The gate was made of 0.4 mm thick stainless steel, and protruded up to 115 mm above the incline. The gate was retracted in about 40 ms by a Nylon string connected by a pulley system to a falling weight.

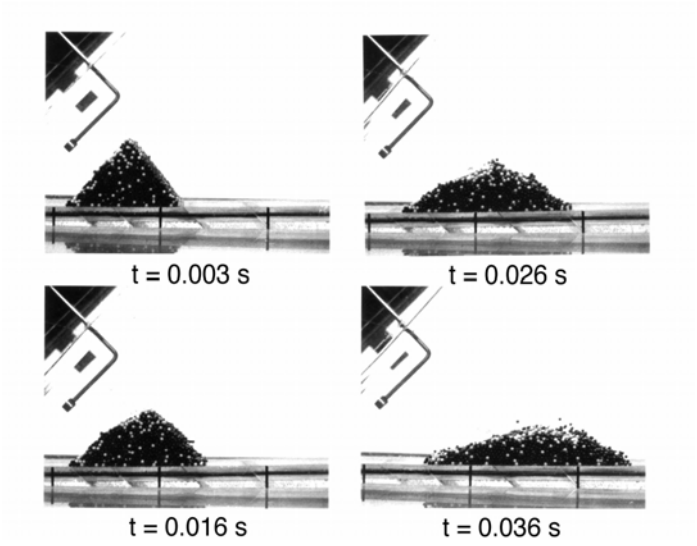

Fig. 2: Steel shot slide frames with tilted camera and wave gauge. The inline is at 45 degrees and the camera was tilted by the same angle.

All granular material experiments were recorded with a high-speed camera that enabled shape, motion, and deformation to be measured (Watts, 1997). Fig. 2 provides four frames from steel shot trial 81, where a small fraction of the steel shot had been painted white in order to document internal slide deformation, and where the camera has been tilted 45 degrees to make the incline look horizontal. The elapsed time from complete gate retraction is indicated, and a wave gauge is visible above the slide in the upper left hand corner. The first frame reveals the slide mass more or less in its initial position, only slightly perturbed by gate retraction. Subsequent frames reveal a rapid downslope spreading along with concomitant thinning as the mass accelerates. The material slide shape, center of mass motion, and deformation were found by tracing the slide outline from the high-speed movie frames. For a typical slide, every third or fourth frame was traced with the first trace occurring before the trial began. Four registry marks were spaced 101.6 mm (four inches) apart along the outside of the incline and some are visible on Fig. 2. The black and white image was scanned to a PICT file and imported into NIH Image 1.61 software in order to process the image. The centroid calculated by NIH Image for a slide trace assumed that the mass was evenly distributed throughout the cross-sectional profile. For early times and for materials with large particles, the assumption of a uniform solid volume fraction throughout

the slide profile appeared to be valid.

NUMERICAL EXPERIMENT METHODS

Numerical experiments are convenient because of the ease with which the user can control model inputs and measure simulation outputs. In addition, it is often quicker and cheaper to explore a parameter space with numerical experiments than it is to do similar work with laboratory experiments. However, a number of choices must be made, including the type of model, the implementation of the model, the base case of interest, and the size of the parameter space of interest.

Table 2. Input parameters for the numerical experiments with SI units

Trial	S_u	ρ_b	T	θ	B
2	2000	1900	100	5°	10000
4	1000	1900	100	5°	10000
5	4000	1900	100	5°	10000
6	2000	1600	100	5°	10000
7	2000	2200	100	5°	10000
8	2000	1900	75	5°	10000
9	2000	1900	125	5°	10000
10	2000	1900	100	4°	10000
11	2000	1900	100	6°	10000
1	200	1900	10	5°	1000
3	20000	1900	1000	5°	100000

We chose to model underwater slides with BING version 1.3, in part because it is a widely used and comparatively simple model with which to demonstrate our techniques (see Imran *et al.*, 2000, 2001). We note here that BING is not constrained to only planar slopes. For our implementation, we chose the Herschel-Bulkley constitutive relation with an exponent of unity, which reduces to the familiar Bingham plastic behavior employed by the landslide model of Jiang and LeBlond (1993). We simulated all underwater slides with 276 nodes, a reference strain rate of 5, and an ambient fluid density of 1000 kg/m^3. Our base case corresponds to trial 2 listed in Table 2, which also lists the inputs for the 10 other numerical experiments. The base case comprises a presumably realistic and tsunamigenic underwater slide. This particular base case may yield underwater slide behaviors that are not representative of events with considerably different size or shape.

Table 3. Dimensionless parameters of the numerical experiments

Trial	θ	γ	T/B	C_n
2	5°	1.9	0.0100	0.0034
4	5°	1.9	0.0100	0.0017
5	5°	1.9	0.0100	0.0068
6	5°	1.6	0.0100	0.0051
7	5°	2.2	0.0100	0.0025
8	5°	1.9	0.0075	0.0045
9	5°	1.9	0.0125	0.0027
10	4°	1.9	0.0100	0.0034
11	6°	1.9	0.0100	0.0034
1	5°	1.9	0.0100	0.0034
3	5°	1.9	0.0100	0.0034

The parameter space covered apart from our base case is best considered with dimensionless quantities. Among other things, Table 3 indicates that numerical experiments 1 and 3 are identical to our base case in this parameter space, even though the slide length changes by an order of magnitude. Also, a quick calculation reveals that gravitational forcing $(\sin\theta)$ is at least an order of magnitude greater than Coulomb friction $(C_n \cos\theta)$. We must assume that all other model coefficients, including any added mass or drag coefficients, remain constant. Last of all, we apprise the reader that we cannot run BING simulations of our laboratory experiments, because BING makes the small angle approximation $\sin\theta \approx \theta$, and because BING assumes a parabolic initial slide profile, quite different from the initial shape in Fig. 2. We integrate over the slide volume to find the center of mass.

LABORATORY EXPERIMENT RESULTS

We follow Watts (1997) and demonstrate that the analytical form describing material slide center of mass motion corresponds to that of a solid block slide, that is Eq. 1. Fig. 3 shows the center of mass position of the 3 mm steel shot slide as a function of time along with a curve fit of Eq. 1. The curve fit has an r^2 value of 0.9998. All other center of mass position data produced similar curve fit results. Given the accuracy of the curve fit, we can use the results from the curve fit to extract a characteristic distance s_o and a characteristic duration t_o of material slide motion. The second and third columns in Table 4 summarize the results of the curve fits of slide center of mass position along the incline as a function of time.

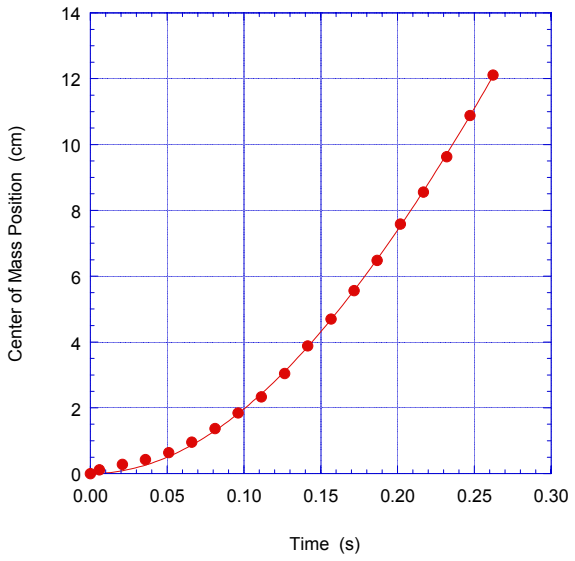

Fig. 3: Curve fit of Eq. 1 with steel shot slide center of mass position

All material slides experienced an initial drop in the center of mass height H perpendicular to the incline. In general, the center of mass drop was linear in time

$$H(t) \approx H_o - U t \qquad (7)$$

for sufficiently early times, such as those considered here. Fig. 4 shows the drop in height perpendicular to the incline as a function of time for

the 3 mm steel shot slide. A linear curve fit over all height measurements yields the dimensionless drop rate listed in Table 4. The linear curve fit has an r^2 value of 0.9862. There is an s-shaped secondary structure within the data of Fig. 4 that suggests a nonlinear behavior at longer times. The drop rate U appears to depend on the material density more than any other material characteristic. It is the component of gravitational forcing normal to the incline that is primarily responsible for the spreading of material slides at short times. The gravitational forcing is in turn proportional to the landslide mass or driving force, and therefore must be related to center of mass motion.

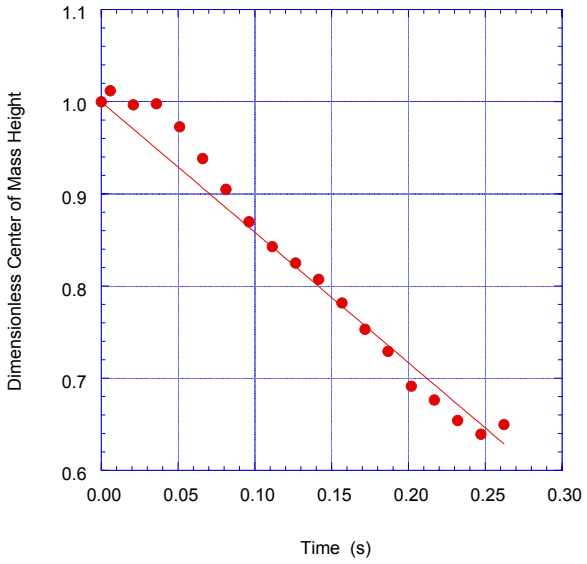

Fig. 4: Curve fit of Eq. 7 with steel shot slide center of mass height

These experiments were conducted with slides of similar size, similar shape, similar particle diameters, and similar friction coefficients on the same 45 degree slope. Therefore, the only slide parameter with any appreciable variation was the bulk density, or specific gravity. While center of mass motion equations such as Eqs. 2-5 already account for changes in bulk density, we have not yet accounted for any influence that bulk density may have on slide deformation. As we have already noted, slide deformation can influence center of mass motion, and therefore it can modify the characteristic distance s_o and characteristic duration t_o of motion at early times. The triangular initial shape also modifies Eq. 3 by a small numerical factor (Watts, 1998).

Table 4. Actual measured (A) and predicted theoretical (P) slide center of mass motion, for laboratory experiments

Material	s_o (cm) (A)	t_o (s) (A)	$U t_o / H_o$ (A)	s_o (cm) (P)	t_o (s) (P)
Glass	17.1	0.324	0.150	13.4	0.251
Steel	29.5	0.271	0.492	29.6	0.262
Lead	38.4	0.295	0.836	70.6	0.408

These facts allow us to relate the ratio of observed characteristics of motion s_o and t_o to those predicted by Eqs. 2-5, to the specific density γ. We have modified Eq. 3 appropriately. From columns 5 and 6 in Table 4, we find that the glass beads have characteristics of motion about 30% larger than predicted, that the steel shot has similar characteristics of motion as those predicted, and that lead shot has smaller characteristics of motion than predicted. These results indicate a complicated mechanics within the slide mass proper.

NUMERICAL EXPERIMENT RESULTS

For our numerical experiments with BING, we also find that the center of mass motion of a deforming slide conforms to Eq. 1. Fig. 5 shows a curve fit of center of mass position as a function of time for our base case. The curve fit has an r^2 value of 0.9999. The curve fitting results for all numerical experiment are listed in Table 5. The functional form of the center of mass motion appears to remain the same, whether or not a slide deforms, and whether results are from laboratory or numerical experiments of deforming slides. We note the value $t_o = 306$ s from Table 5 in order to prove that the times shown on Fig. 5 do in fact span our definition of early times. In addition, the final experimental point shown on Fig. 5, which occurs at a time $t > t_o$, corresponds to the maximum slide velocity. Afterward, the center of mass begins to slow down. BING therefore predicts sufficient time for complete tsunami generation along a planar slope.

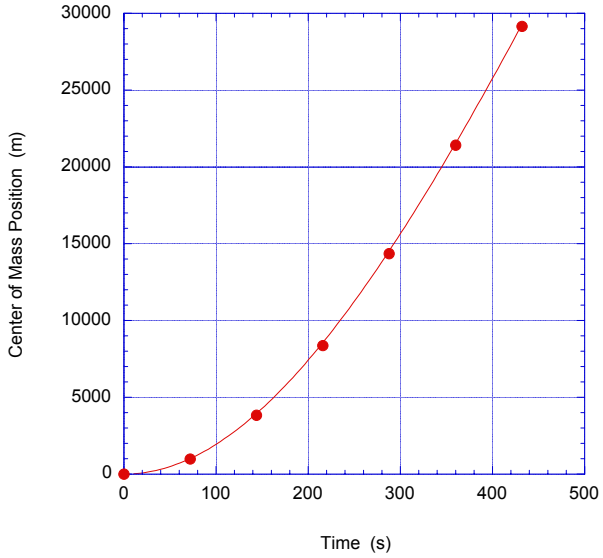

Fig. 5: Curve fit of Eq. 1 with model base case center of mass position

The evolution of maximum slide thickness in Fig. 6 also follows a predictable pattern, with thickness dropping linearly in time. The curve fit has an r^2 value of 0.9927 on account of a secondary structure within the data. There is a consistent s-shaped structure about the linear drop, with the thickness decreasing slower than average at first, then faster than average, and finally with an indication that the decrease is slowing down at later times. This behavior makes sense, because we know that the thickness must eventually reach a finite asymptote when the slide comes to rest, but this occurs at later times than those shown. The behavior was noted on Fig. 4 for the granular material slides and may be general. The data in Fig. 6 are at the same times as those in Fig. 5.

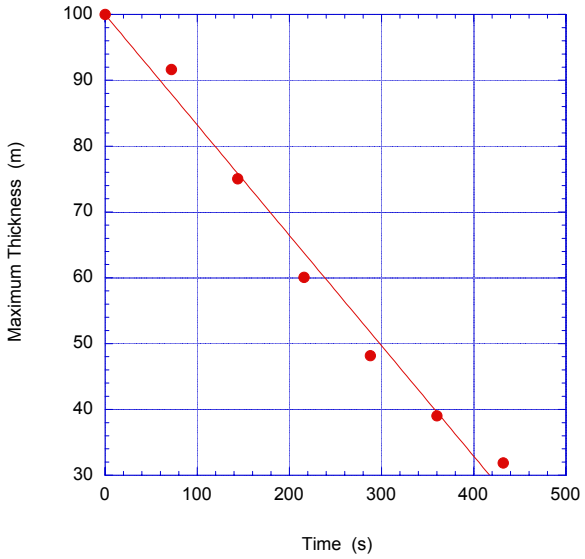

Fig. 6: Linear curve fit of model base case maximum thickness in time

The instantaneous slide length is a difficult quantity to define because we do not want to include solidified sediment in the slide tail. We define a typical slide length based on its volume V and maximum thickness T as $B = 3V/2T$ by assuming that the slide remains more or less a parabolic profile. Our definition has the advantage of reproducing the correct initial slide length entered into BING. Fig. 7 shows the typical length increasing in direct proportion to the distance traveled by the center of mass. The linear curve fit has an r^2 value of 0.9992. Slides therefore possess a direct relationship between the center of mass motion and deformation about the center of mass.

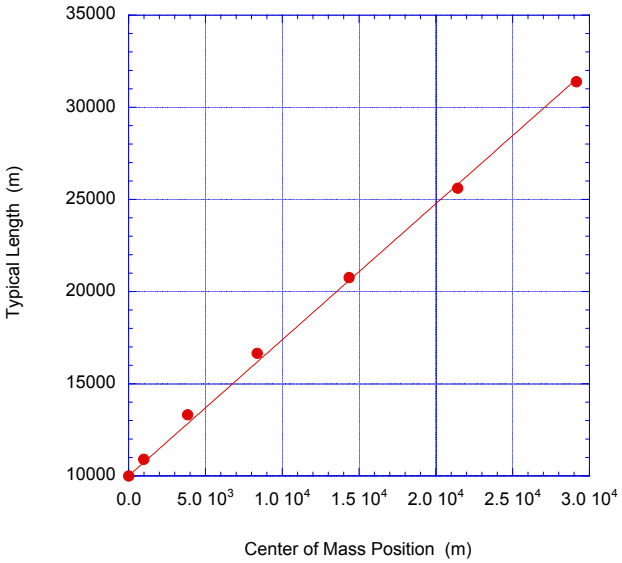

Fig. 7: Linear curve fit of model base case typical length

The nose position in Fig. 8 follows the same pattern as that of typical length in Fig. 7, with the nose position increasing in direct proportion to the distance traveled by the center of mass. The linear curve fit has an r^2 value of 0.9998. The slopes found from the linear curve fits are all indicated in Table 5. We note that the slope $m_{thickness}$ has units of length over time because of the *ad hoc* nature of that specific curve fit.

Table 5. Actual results from the numerical experiments with BING

Trial	s_o (m)	t_o (s)	$m_{thickness}$	m_{length}	m_{nose}
2	37330	306	-0.168	0.738	1.32
4	66904	410	-0.152	0.670	1.32
5	28928	282	-0.173	0.820	1.33
6	34983	342	-0.148	0.789	1.35
7	54213	348	-0.176	0.713	1.32
8	33797	299	-0.116	0.670	1.31
9	54395	374	-0.211	0.808	1.36
10	37781	352	-0.158	0.878	1.38
11	51286	332	-0.170	0.647	1.30
1	2065	73	-0.054	0.820	1.34
3	910610	1554	-0.470	0.670	1.32

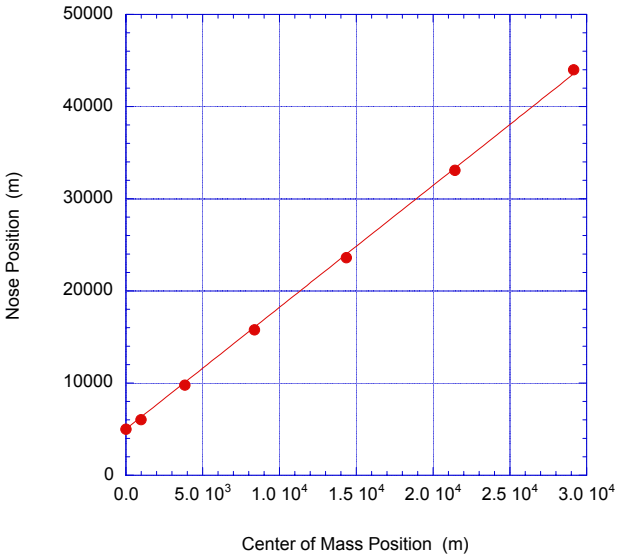

Fig. 8: Linear curve fit of model base case nose position

We find that our chosen numerical experiments produce reasonably consistent values for the slide features considered here. To make our point more clearly, we provide the means and standard deviations for all quantities in Table 5, excluding trials 1 and 3 which are only similar for dimensionless quantities. We obtain the characteristic distance of motion s_o = 44402 ± 12670 m, the characteristic duration of motion t_o = 338 ± 39 s, the slope $m_{thickness}$ = -0.164 ± 0.026 m/s, the slope m_{length} = 0.748 ± 0.080, and the slope m_{nose} = 1.332 ± 0.025. It is clear that most quantities have standard errors of 10% or less, indicating a high degree of predictability. This fact is all the more

surprising because the different input parameters in Tables 2 and 3 span a variation of at least 20-30%. Therefore, the numerical model BING has actually reduced the sensitivity of our chosen output results relative to the input parameters.

DISCUSSION

We divide our discussion into an examination of our experimental results, and then considerations of tsunami generation.

Slide Shape, Motion, and Deformation

Watts (1997) and Watts *et al.* (2000) demonstrated that the center of mass motion of deforming slides could be described by Eq. 1 at early times. We suggest in this work that these previous results may be general, and apply both to center of mass motion and to slide deformation. The fact that underwater slides have a predictable center of mass motion suggests that the force balance used to derive Eq. 1 remains valid on the scale of the entire slide, regardless of the internal deformations experienced locally by the slide. One explanation lies in the observation that densely packed arrays of particles several monolayers thick are observed in Fig. 2 sliding along the incline in the bulk of the slide (Watts, 1997). A similar explanation is that slide deformation may not alter appreciably the values of the dynamical coefficients acting on the slide mass. Therefore, solid block values of these coefficients remain relevant to deforming slides. Regardless, it appears possible to describe center of mass motion despite the mechanical details internal to a landslide model.

Table 6. Ratio of actual to predicted (Eqs. 2-5) results of numerical experiments with BING

Trial	s_o ratio	t_o ratio	u_t ratio	a_o ratio
2	1.12	0.75	1.34	1.97
4	2.00	1.02	1.65	1.93
5	0.87	0.68	1.06	1.87
6	1.14	0.74	1.31	2.08
7	1.50	0.92	1.34	1.78
8	1.01	0.73	1.18	1.89
9	1.63	0.92	1.48	1.91
10	1.13	0.77	1.26	1.90
11	1.54	0.90	1.42	1.91
1	0.62	0.56	1.00	1.94
3	2.73	1.21	1.73	1.87

Consequently, Eq. 1 can be viewed as a canonical description of slide center of mass motion at early times. We have yet to find any fundamental reason why slide thickness would decrease linearly in time at early times. However, we consider the linear drop in thickness to be sufficiently accurate so as to be useful in studies of tsunami generation. It is clear that this functional form cannot remain valid at later times, so this is not a general result of slide dynamics. The fact that slide length increases with distance traveled suggests that center of mass motion is the driving force for slide deformation. In retrospect, there seems to be no alternative to describe how slide length increases, because the only other dynamic length scale is the center of mass position. The ratio of these two length scales apparently forms a constant dimensionless quantity, because this is the only way that the dimension of length could arise that describes changes in the typical slide length. Consequently, this result may be fundamental to slide deformation at early times, although the numerical coefficient may vary. A similar result is found for the position of the slide nose, which supports our contention, once again, that the center of mass position is a fundamental measure of slide deformation.

Table 6 provides ratios of actual to predicted quantities in order to test the significance of solid block center of mass equations over the entire parameter space of the numerical experiments. In general, we find that all of the ratios are of order unity, indicating that solid block center of mass equations can account for most first-order effects produced by BING. The characteristic distance of center of mass motion does not depend on deformation about the center of mass. The mean ratio is 1.326 ± 0.362 at one standard deviation. The characteristic duration of center of mass motion tends to be smaller than predicted, indicating a more rapid approach to a maximum velocity. The mean ratio is 0.826 ± 0.330. Our maximum velocity results are basically a consequence of the scaling of slide velocity with the square root of slide length. For trial 1 we find $u_{\max} = 26$ m/s, for trial 2 we find $u_{\max} = 110$ m/s, and for trial 3 we find $u_{\max} = 450$ m/s. We contend that other solutions of Newton's equations of motion will confirm that our slide velocities are correct. Once again, the center of mass maximum velocity does not depend on slide deformation. The mean ratio of actual maximum to theoretical terminal velocity is 1.336 ± 0.172. Last of all, we find that the initial acceleration of the center of mass has been almost doubled on account of the rapid shifting of mass towards the front of the slide at early times. The mean ratio is 1.916 ± 0.080. Watts *et al.* (2000) found a similar result, and suggested that the increased acceleration may enhance tsunami generation.

Tsunami Generation Considerations

We have focused so far in this paper on underwater slide shape, motion, and deformation, with the goal of applying these results to tsunami generation. The available space permits a qualitative consideration that builds upon the results presented above. Despite these limitations, we draw conclusions with potentially significant bearings on landslide tsunami hazard assessment.

Watts (1997) found experimentally that there is no significant change in center of mass motion related to deformable slides, nor is there any apparent change in tsunami wavelength associated with deformation. Deformation about the center of mass does not appear to alter the fundamental physics described by Wiegel (1955) or Watts (1998, 2000). Consequently, solid block motion is representative of deforming slide motion, and solid block tsunami generation should also be representative of deforming slide tsunami generation.

Our research to date suggests that deformation about the total center of mass motion appears so far to have little tsunamigenic importance. That is, the precise shape of a slide may not be a major factor in tsunami generation, although research is continuing on this matter. The basic issue is that a decrease in thickness over time will decrease tsunami generation, whereas an increase in the initial acceleration will increase tsunami generation, both acting at the same time. With these competing effects, it is not clear how tsunami amplitude would be affected by deformation. Some tsunami generation models (e.g., Jiang and LeBlond 1992, 1993, 1994) have emphasized slide deformation, but current users seem to skip "relative motion" altogether and assume that the deformation itself is fundamentally tsunamigenic. The problem here is that the water wave model of Jiang and LeBlond (1992, 1993, 1994) will always make deformation look important, because the shallow water wave assumption forces the free surface to mimic vertical bottom accelerations. Consequently, a more sophisticated tsunami generation model may be needed to resolve these issues.

Underwater landslide velocities in the range of 50-70 m/s are common values for destructive landslides, but it is also true that smaller landslides are more common than larger events. We have shown that researchers need to be careful, because maximum velocity depends on landslide size. This fact enables slides of initial length of order O(10 km) to achieve maximum velocities that are significantly greater than commonly accepted. A typical long wave celerity in the open ocean is 220 m/s, and an underwater slide with this velocity provides an instantaneous Froude number of unity (Fr=1). Our analyses suggest that such a condition can be achieved in nature. In general, when a moving body matches the wave speed, wave amplitudes can be expected to grow rapidly (Tinti and Bortolucci, 2000). However, we are most interested in the far-field behavior of such a wave. We consider our maximum velocity result along with the work of Ben-Menahem and Rosenman (1972) as well as that of Iwasaki (1997) in order to describe tsunami propagation in a qualitative manner. Under the condition of Froude number close to unity, landslide tsunamis would be capable of beaming focused energy into the far field as if the water waves were "bullets" originating from a landslide "rifle". It therefore appears to us as if landslide tsunamis can sometimes generate transoceanic hazards.

CONCLUSIONS

We have presented experimental and numerical results that suggest general behaviors of tsunamigenic underwater slide shape, motion and deformation at early times. These behaviors have direct consequences on the tsunamigenic potential of underwater slides. With a surprising degree of consistency and accuracy, we document motion and deformation that can be described and scaled with theoretical predictions derived for solid blocks. Our experimental work presents a granular mass moving and deforming down a steep incline. Our numerical work uses BING to simulate more realistic underwater slide models. Regardless of the system being studied or the techniques employed, we find that it is possible to reduce our results into simple analytical expressions of slide shape, motion, and deformation. We do not develop particular analytical expressions for this work, which is mostly presented in tabular form, although curve fits of our results are readily performed. Instead, the technique that we developed is presumably general in nature. We conjecture that almost all experimental or numerical work on underwater slides can be reduced in a similar manner, perhaps with different curve fit results or numerical coefficients. In this work, we sacrifice the precision learned through reductive models in return for approximate descriptions of coherent slide features. Because our expressions capture only specific coherent features of underwater slides, there will always be a role for more reductive experiments and simulations.

ACKNOWLEDGEMENTS

PW received support for doctoral studies from the US National Science Foundation through grant CMS-9523414 to Fred Raichlen at the California Institute of Technology. The remainder of this work was supported by the US National Science Foundation under research grant CMS-0100223 made to STG at the University of Rhode Island.

REFERENCES

Assier-Rzadkiewicz, S, Mariotti, C, and Heinrich, P (1997). "Numerical Simulation of Submarine Landslides and their Hydraulic Effects," *J Wtrwy, Port, Coast, and Oc Eng*, ASCE, Vol 123, No 4, pp 149-157.

Ben-Menahem, A, and Rosenman, M (1972). "Amplitude Patterns of Tsunami Waves from Submarine Earthquakes," *J Geoph Res*, Vol 77, pp 3097-3128.

Edgers, L, and Karlsrud, K (1982). "Soil Flows Generated by Submarine Slides: Case Studies and Consequences," *Nor Geotech Inst Bull*, Vol 143, pp 1-11.

Grilli, ST, and Watts, P (1999). "Modeling of Waves Generated by a Moving Submerged Body: Applications to Underwater Landslides," *Eng Analysis with Boundary Elements*, Vol 23, No 8, pp 645-656.

Grilli, ST, and Watts, P (2001). "Modeling of Tsunami Generation by an Underwater Landslide in a 3D Numerical Wave Tank" *Proc of the 11th Offshore and Polar Eng Conf*, ISOPE01, Stavanger, Norway, Vol 3, pp 132-139.

Grilli, ST, Vogelmann, S, and Watts, P (2002). "Development of a 3D Numerical Wave Tank for Modeling Tsunami Generation by Underwater Landslides," *Eng Analysis with Boundary Elements*, Vol 26, No 4, pp 301-313.

Hampton, MA, Lee, HJ, and Locat, J (1996). "Submarine Landslides," *Rev Geophys*, Vol 34, No 1, pp 33-59.

Imamura, F, and Imteaz, MMA (1995). "Long Waves in Two-layers: Governing Equations and Numerical Model," *Sci Tsunami Hazards*, Vol 13, pp 3-24.

Imran, J, Harff, P, and Parker, G (2000). "A Numerical Model of Submarine Debris Flow with Graphical User Interface," *Computers and Geosciences*, Vol 27, pp 717-729.

Imran, J, Parker, G, Locat, J, and Lee, H (2001). "1D Numerical Model of Muddy Subaqueous and Subaerial Debris Flow," *J Hyd Eng*, ASCE, Vol 127, No 11, pp 959-968.

Iwasaki, S (1997). "The Wave Forms and Directivity of a Tsunami Generated by an Earthquake and a Landslide," *Sci Tsunami Hazards*, Vol 15, pp 23-40.

Jiang, L, and LeBlond, PH (1992). "The Coupling of a Submarine Slide and the Surface Waves Which it Generates," *J Geoph Res*, Vol 97, pp 12731-12744.

Jiang, L, and LeBlond, PH (1993). "Numerical Modeling of an Underwater Bingham Plastic Mudslide and the Waves Which it Generates," *J Geoph Res*, Vol 98, pp 10303-10317.

Jiang, L, and LeBlond, PH (1994). "Three-dimensional Modeling of Tsunami Generation due to a Submarine Mudslide," *J Phys Ocean*, Vol 24, pp 559-573.

Pelinovsky, E, and Poplavsky, A (1996). "Simplified Model of Tsunami Generation by Submarine Landslide," *Phys Chem Earth*, Vol 21, No 12, pp 13-17.

Prior, DB, and Coleman, JM (1979). "Submarine Landslides: Geometry and Nomenclature," *Z Geomorph N F*, Vol 23, No 4, pp 415-426.

Schwab, WC, Lee, HJ, and Twichell, DC (1993). "Submarine Landslides: Selected Studies in the U.S. Exclusive Economic Zone," *US Geol Surv Bull 2002, US Dept. of Interior, Washington, DC*.

Tinti, S, and Bortolucci, E (2000). "Energy of Water Waves Induced by Submarine Landslides," *Pure Appl Geophys*, Vol 157, pp 281–318.

Watts, P (1997). "Water Waves Generated by Underwater Landslides," *PhD thesis, California Inst of Technol, Pasadena, CA*.

Watts, P (1998). "Wavemaker Curves for Tsunamis Generated by Underwater Landslides," *J Wtrwy, Port, Coast, and Oc Eng*, ASCE, Vol 124, No 3, pp 127-137.

Watts, P (2000). "Tsunami Features of Solid Block Underwater Landslides," *J Wtrwy, Port, Coast, and Oc Eng*, ASCE, Vol 126, No 3, pp 144-152.

Watts, P, Imamura, F, and Grilli, ST (2000). "Comparing Model Simulations of Three Benchmark Tsunami Generation Cases," *Sci Tsunami Hazards*, Vol 18, No 2, pp 107-124.

Wiegel, RL (1955). "Laboratory Studies of Gravity Waves Generated by the Movement of a Submarine Body," *Trans Am Geophys Union*, Vol 36, No 5, pp 759-774.